THE JOURNAL OF PHYSICAL CHEMISTRY C

Article

Cite This: J. Phys. Chem. C 2019, 123, 22812−22822

pubs.acs.org/JPCC

Ab Initio Investigation of Li and Na Migration in Guest-Free, Type I Clathrates

Andrew Dopilka,[†] Xihong Peng,*[,‡] and Candace K. Chan*[,†]

[†]Materials Science and Engineering, School for Engineering of Matter, Transport and Energy, Arizona State University, P.O. Box 876106, Tempe, Arizona 85827, United States

[‡]Science and Mathematics, College of Integrative Sciences and Arts, Arizona State University, Mesa, Arizona 85212, United States

Supporting Information

ABSTRACT: Guest-free, type I clathrates with formula Tt_{46} (Tt = Si, Ge, Sn) are comprised of open, cage-like frameworks with the potential for facile Li or Na conduction. Herein, ab initio density functional theory (DFT) is used to evaluate the ionic mobility of Li and Na through the clathrate crystal structures. The favorable Li and Na positions inside the clathrate structures are determined, and the migration pathways and barriers are evaluated using the nudged elastic band (NEB) method. The results show that it is energetically favorable for a Li atom to occupy the center position inside the small Tt_{20} cages while preferring the off-center positions in the larger Tt_{24} cages. The lowest Li migration barriers are found to be 0.35, 0.13 and 0.37 eV for Si_{46}, Ge_{46}, and Sn_{46}, respectively, with the dominant diffusion pathway along channels of Tt_{24} cages connected by hexagonal faces. Li accessibility to the Si_{20} cage in Si_{46} appears to be restricted in the dilute regime due to a high energy barrier (2.0 eV) except for the case in which Li atoms are present in adjacent cages; this lowers the migration barrier to 0.77 eV via a mechanism where a Si−Si bond is temporarily broken. In contrast, Na atoms show preference for the cage centers and display higher migration barriers than Li. Overall, the Tt_{24} channel sizes in the guest-free, type I clathrates are ideal for fast Li diffusion, while Na is too large to migrate effectively between cages. The energy landscape for Li inside the type I clathrates is uniquely different than that in diamond cubic structures, leading to significantly lower energy barriers for Li migration. These results suggest that open frameworks of intermetallic elements may enable facile Li migration and have potential use as Li-ion battery anodes.

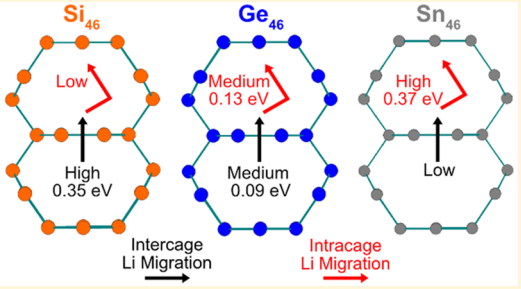

1. INTRODUCTION

To meet the stringent power and energy density requirements for next-generation batteries, there has been considerable attention given to the search for materials with high ionic mobility, an important connection to the diffusion coefficient, which contributes to the rate capability of a battery electrode. The energy landscape of the migrating ion is a key factor in determining the ionic mobility in solid materials. In general, fast ion conductors are characterized by diffusing ions in a "frustrated" or flat energy landscape, where there is considerable disorder on the intercalant sites, leading to small kinetic barriers for transport.[1,2]

Intermetallic clathrates have cage structures that host guest atoms and exhibit interesting characteristics including superconductivity,[3−7] hydrogen storage,[8,9] tunable optical properties,[10] and thermoelectricity.[11−16] The origin of such properties is the unique interaction between the sp^3-bonded host framework with the guest atoms and the defects associated with this structural type. Recently, there has been much interest in the mobility of ions within clathrates and the potential of this class of materials to be used as anodes in lithium-ion batteries.[17−26] However, further investigation is needed to identify the structural features of the unique cage framework that are suitable for ion conduction. Understanding the mobility of guest atoms within clathrates is relevant not only for battery insertion electrodes that rely on bulk ion diffusion but also for the synthesis of clathrates and other novel polymorphs[27] (e.g., Si_{136},[28−30] Si_{24},[31] Si_6H_6,[32] Ge_{136},[10,33] allo-Ge,[34] germanane[35]), where removal of the alkali metal guests via thermal evaporation or oxidative deintercalation at the surface is a possible path to obtaining the desired structures.

Our group has thoroughly investigated the electrochemical reactions of Tetrel (Tt) clathrates with Li and found that type I clathrates based on Ba_8Tt_{46} (Tt = Si, Ge) do not intercalate Li atoms, with the observed reactions mainly confined to the surface or occurring through bulk, electrochemically induced conversion processes to amorphous phases.[20,25,26] In our recent study on Ba_8Ge_{43} clathrates, density functional theory (DFT) calculations suggested that it was energetically feasible for Li to occupy vacancies on the framework sites, but the migration energy barrier between them was found to be too high for room temperature lithiation due to the presence of Ba atoms in the cages.[26] If the Ba atom was absent, the calculated

Received: July 6, 2019
Revised: August 25, 2019
Published: August 28, 2019

DOI: 10.1021/acs.jpcc.9b06424
J. Phys. Chem. C 2019, 123, 22812−22822

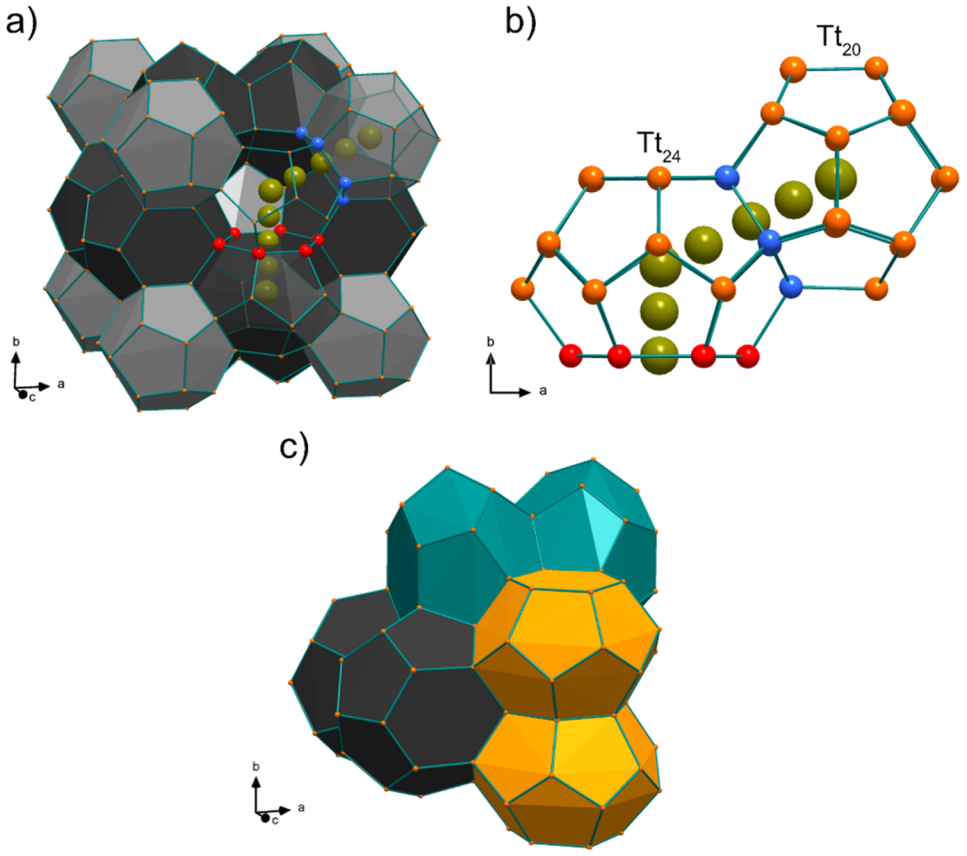

Figure 1. Crystal structures of type I clathrate Tt_{46}. Orange atoms represent Tt framework atoms (Tt = Si, Ge, Sn). Olive-colored atoms represent the positions of the M guest atom (M = Li, Na) as it migrates through Tt atoms in the hexagonal and pentagonal faces between connected cages (indicated by red and blue atoms, respectively). (a) Polyhedral view, with the black polyhedra representing the tetrakaidecahedra (Tt_{24} cages) and the gray polyhedra representing the dodecahedra (Tt_{20} cages). (b) Ball-and-stick view of a Tt_{24} and Tt_{20} cage viewed down the [001]. (c) Polyhedral view with the three perpendicular channels of interconnected Tt_{24} cages (i.e., via connected hexagons) shaded in different colors.

migration barrier decreased dramatically, suggesting the need for guest atom vacancies to enable Li migration.

To further investigate the mobility of ions in clathrates, herein we use first-principles DFT methods to calculate the migration pathways of Li and Na in guest-free, type I clathrates Tt_{46} (Tt = Si, Ge, and Sn) and to explore how the energy barrier varies with the type of framework atom. The preferred Li and Na atom positions were calculated based on the Gibbs free energy change of reaction; the nudged elastic band (NEB) method was used to estimate migration barriers for different pathways within and between cages to evaluate the ionic mobility. We find that Li migration in guest-free, type I clathrates is accompanied by low energy barriers comparable to those in state-of-the-art Li-ion conductors, which suggests the possibility of facile Li migration through the clathrate frameworks. This is attributed to the destabilization of Li in the large Tt_{24} cages, since the lowest energy sites are not in the center of the cage cavity, resulting in considerable disorder. The energy barrier is dependent on the cage size, with Ge_{46} displaying the lowest Li migration barrier of 0.13 eV. For Na migration, the migration barriers are significantly higher between cages, suggesting limited Na mobility through the clathrate frameworks. These results will help guide researchers in the design and experimentation of clathrates and other open framework intermetallic compounds as potential anodes for Li- and Na-ion batteries.

2. COMPUTATIONAL METHODS

The first-principles DFT calculations were performed to explore Li (Na) insertion and migration in guest-free type I clathrates using a similar manner as in our previous work.[21,26] The calculations were carried out using the VASP code,[36,37] the PBE functional,[38] and projector augmented wave (PAW) potentials with a plane wave basis set.[37] In the PAW potentials, the Si 3s and 3p, Ge 4p and 3d, Sn 5p and 4d, Li 1s and 2s, Na 3s and 2p, Mg 3s and 2p, and Ba 5s and 5p electrons were treated as valence electrons. The kinetic energy cutoff for the plane wave basis set was chosen to be 400 eV, and the reciprocal space was sampled with the Monkhorst pack meshes $3 \times 3 \times 3$ centered at Γ. The cubic Tt_{46} unit cell ($Pm\bar{3}n$ space group) was used in all calculations. The convergence criteria for the electronic and ionic relaxations were set to be 0.01 and 0.1 meV, respectively. These criteria resulted in relaxed structures with residual forces below 0.03 eV/Å. The geometric optimization was performed in two steps. First, the unit cell volume was optimized without the constraint of the cubic symmetry. Then the relaxed lattice constant, taken from the relaxed volume, was used in a second step where only ionic relaxation was allowed under the cubic symmetry constraint. The crystal structures with the ionic positions of the second step are reported.

The Gibbs free energy change of reaction (ΔG_r) and the average voltage were calculated as described previously.[21,26] The formulas used for calculating the Gibbs free energy change

DOI: 10.1021/acs.jpcc.9b06424
J. Phys. Chem. C 2019, 123, 22812−22822

and average voltage for insertion of Li in Tt_{46}, for example, are shown in eqs 1 and 2, respectively

$$\Delta G_r = E(\mathrm{LiTt_{46}}) - E(\mathrm{Li}) - E(\mathrm{Tt_{46}}) \quad (1)$$

$$V(x) = -\frac{\Delta G_r}{x}, \quad x = \text{no. of Li} \quad (2)$$

where $E(\mathrm{LiTt_{46}})$ and $E(\mathrm{Tt_{46}})$ are the total free energies for the clathrate systems with and without the Li atom and $E(\mathrm{Li})$ is the energy per atom for Li metal. The calculated values for $E(\mathrm{Li})$ and $E(\mathrm{Na})$ are −1.904 and −1.311 eV/atom, respectively. A negative ΔG_r (i.e., positive voltage) represents a spontaneous reaction relative to Li (or Na) metal, suggesting the feasibility of lithiation (sodiation) in a half cell with Li (Na) metal as the counter electrode. The formation energies for the clathrate structures were obtained using the equations described in our previous work.[21,26] The elemental energies used for Si, Ge, and Sn were −5.419, −4.621, and −3.912 eV/atom from the diamond cubic (Si, Ge) and tetragonal (Sn) structures. All crystal structure figures were created with Diamond 4.5.3, and movies were created with Jmol.[39]

The climbing image nudged elastic band (NEB) method was used to calculate the Li and Na migration barriers.[40] All NEB calculations used a linear interpolation as a starting band with 7 intermediate images between the beginning and the ending images. The images were converged until the force on each image was below 0.03 eV/Å.

3. RESULTS

3.1. Tt_{46} Structures. The type I clathrate structure crystallizes in the $Pm\bar{3}n$ space group and has a general formula of M_8Tt_{46}, where M is the guest atom hosted inside a framework of Tt (Tt = Si, Ge, and Sn) atoms.[28] The structure is composed of two types of polyhedra, six Tt_{24} (tetrakaidecahedra) and two Tt_{20} (dodecahedra), that host the guest atom, M (Figure 1a). The Tt_{24} cage is composed of 12 pentagonal and 2 hexagonal faces, while the Tt_{20} cage is composed of 12 pentagonal faces. This is highlighted in Figure 1a and 1b, where a hexagon and pentagon are colored in red and blue, respectively. The type I structure can be visualized as one-dimensional (1D) channels of Tt_{24} cages connected by shared hexagonal faces oriented in the three perpendicular directions, while the Tt_{20} cages fill the space between them. This is shown in Figure 1c, where two Tt_{24} in each perpendicular direction are shaded in different colors representing the three 1D channels. The related type II clathrate structure ($Fd\bar{3}m$ space group, general formula $M_{24}Tt_{136}$) is composed of 16 dodecahedral cages (Tt_{20}) and 8 larger hexakaidecahedra (Tt_{28}) in which the Tt_{28} cages are connected in a tetrahedral network via hexagonal faces.[28]

The formation energies and lattice constants of the calculated Tt_{46} structures are presented in Table 1. To our knowledge, there have been no reports on the phase pure synthesis of these empty type I clathrate structures; this is likely due to the distortion of the Tt atoms from the ideal tetrahedral configuration found in their bulk phases. This is supported by the positive formation energies in Table 1, indicating that these structures are metastable with respect to their lower energy, bulk analogues. The lattice constants match well with previous calculations[21,41,42] and their experimental structures (e.g., a = 10.197 Å for Na_8Si_{46}, a = 10.686 Å for K_8Ge_{44}, and a = 12.03 Å for K_8Sn_{44}).[43−45]

Table 1. Formation Energy and Optimized Lattice Constants of the Guest-Free Tt_{46} (Tt = Si, Ge, Sn) Clathrate Structures

composition	formation energy (eV/atom)	lattice constant (Å)
Si_{46}	0.057	10.230
Ge_{46}	0.031	10.720
Sn_{46}	0.152	12.380

3.2. Li Positions in Empty Type I Clathrates. To determine the most favorable lithium sites in the type I clathrate crystal structure, a Li atom was placed in various initial positions in either the Tt_{24} or the Tt_{20} cage of a single Tt_{46} unit cell as described in our previous study.[21] The Gibbs free energy change of reaction (ΔG_r) and corresponding voltage were calculated after relaxation of the unit cell. Figure 2a shows the calculated results for the four Li sites representing

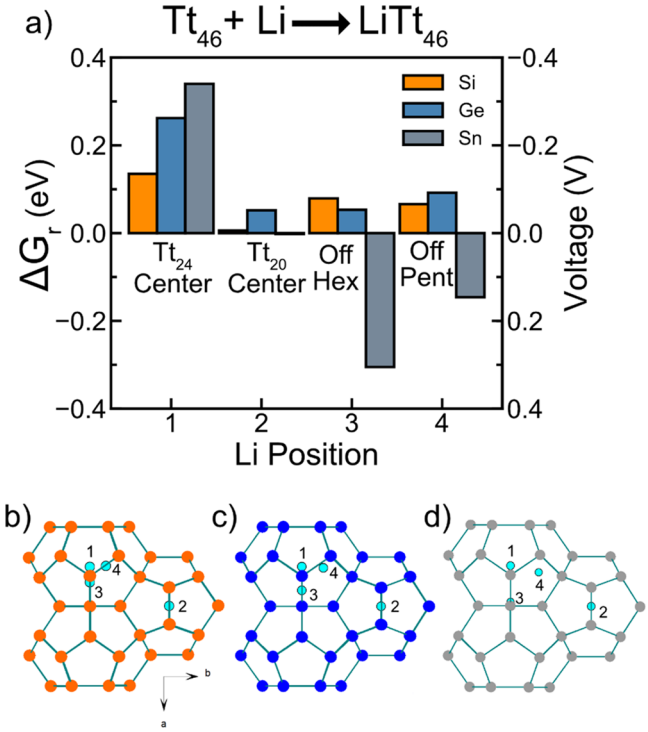

Figure 2. (a) Gibbs free energy change of reaction (ΔG_r) and voltage vs Li/Li^+ for the reaction Tt_{46} + Li → $LiTt_{46}$, where Tt = Si, Ge, and Sn, for each of the 4 Li positions. Schematic with two Tt_{24} cages and one Tt_{20} cage for (b) Si_{46}, (c) Ge_{46}, and (d) Sn_{46} showing the 4 Li positions after relaxation when viewed down the [001] direction. Li = cyan, Si = orange, Ge = blue, Sn = gray.

positions of local minima in the three Tt_{46} structures: (1) the center of the Tt_{24} cage; (2) the center of the Tt_{20} cage; inside the Tt_{24} cage, coordinated off of the (3) hexagonal face (Off Hex) or the (4) pentagonal face (Off Pent). The relaxed Li positions are shown in Figure 2b−d, where the [001] view of two Tt_{24} cages and one Tt_{20} cage is depicted. A negative Gibbs free energy change (positive voltage) indicates a favorable reaction with respect to Li metal, which is a useful metric for predicting whether materials can be electrochemically lithiated in a half-cell with Li metal.

The results show that when a Li atom is relaxed in the Tt_{24} cage center (position 1), ΔG_r is positive and increases when increasing the size of the framework atom (Figure 2a). On the

DOI: 10.1021/acs.jpcc.9b06424
J. Phys. Chem. C 2019, 123, 22812−22822

other hand, it is more favorable for Li to occupy the Tt_{20} cage center (position 2), as indicated by the lower ΔG_r values. This site also has similar energies regardless of the framework atom. On the basis of these results it appears that the size and the geometry/shape of the cage are important for the energetics of the Li insertion sites. The lower energy of the Li position at the Tt_{20} cage center compared to the Tt_{24} center can be attributed to the smaller cage volume and more symmetric cage geometry (since the Tt_{20} cage is made solely of pentagonal faces), which better accommodate the small Li atom. For Sn_{46}, however, we find that Li will prefer an off-center position where it is coordinated by a pentagonal face in the Sn_{20} cage because of the larger cage sizes compared to Si_{46} and Ge_{46} (shown in Figure S1). Indeed, ΔG_r = −0.181 eV for this off-centered position in the Sn_{20} cage, which is much lower than that for the Sn_{20} center position (ΔG_r = −1.6 meV) as well as the Off Pent position in the Sn_{24} cage. From this we can see that Li will still prefer an off-center position if the Tt_{20} cage is large enough.

Considering Li inside a Tt_{24} cage, the results show that for all three Tt_{46} compositions Li prefers to be coordinated off of a hexagonal (position 3, Off Hex) or pentagonal (position 4, Off Pent) face instead of occupying the Tt_{24} cage center. Due to the similar energies of these off-center positions, this suggests that Li inside a Tt_{24} cage will display positional disorder. The Li−Tt bond lengths and lattice parameters for the relaxed structures containing Li in each of the 4 positions are presented in Table S1. For the Off Hex and Off Pent positions for the three Tt_{46} compositions, the Li−Tt distance range was around 2.8−3.0 Å, suggesting that this is the energetically favored Li−Tt bond length. The most favorable Li site in both Ge_{46} and Sn_{46} is position 3 (Off Hex), where Li resides closer to the hexagonal face than the cage center (Figure 2c and 2d). In Sn_{46}, the relaxed Off Hex Li position is very close to the center of the hexagonal face with a Li−Sn distance of 2.90 Å, meaning that the hexagon in Sn_{46} is large enough for Li to favorably reside near the center. For Si_{46}, Li position 4 (Off Pent) is the most favorable site but the energy is only slightly lower (13 and 69 meV, respectively) to those for Li position 3 (Off Hex) and Li position 1 (Tt_{24} Cage center). As the size of the Tt_{24} cage increases from Si to Sn clathrates, not only does the cage center position become more unfavorable but also Li prefers to be coordinated near the hexagonal face instead of the pentagonal one, likely due to the increased amount of interaction with six Tt atoms compared to five. The ΔG_r values for the reaction of Li with Ge_{46} and Si_{46} are both slightly positive, suggesting that these reactions would not be favorable in a half cell with Li metal. A more detailed study investigating the energies of various compositions and considering the ordering of Li would be needed to estimate the exact reaction voltages.[46−48]

3.3. Li Migration Pathways in Empty Type I Clathrates. Because each cage in the clathrate structure is composed of several different faces (pentagonal or hexagonal), the ionic mobility between cages is expected to be impacted by the geometry of these faces. If the initial position of M (M = Li, Na) is near the center of a cage it must traverse through either a hexagonal or a pentagonal face to reach an adjacent cage unless it goes through a Tt−Tt bond. These possible intercage pathways (presented via the atomic positions used in the NEB calculations) are illustrated in Figure 1a and 1b.

The NEB results to evaluate Li mobility within the clathrate structure are presented in Figure 3. Figure 3a shows the NEB calculations for Li migration between two Tt_{24} cages through

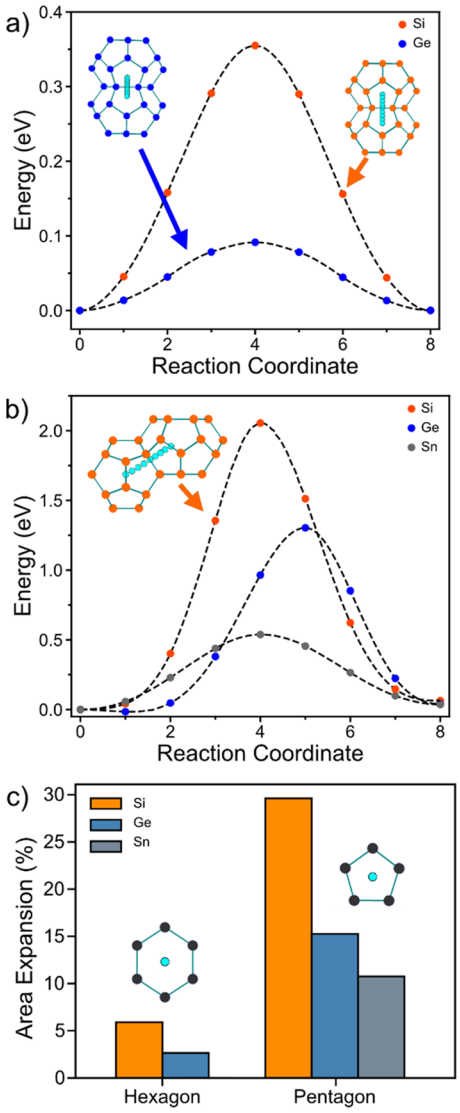

Figure 3. (a) NEB-calculated minimum energy path for Li (cyan) migration in Si_{46} and Ge_{46} between the Off Hex positions in two adjacent Tt_{24} cages through a hexagonal face. (b) NEB-calculated minimum energy path for Li migration between the Tt_{20} and the Tt_{24} cages through a pentagonal face. (c) Percentage of the area expansion of the hexagonal and pentagonal faces at the highest energy position for the two pathways in a and b relative to the starting size of the hexagon/pentagon.

the interconnecting hexagonal face for Tt = Si and Ge (Tt = Sn is not included because the center of the hexagon is a local energy minimum in $LiSn_{46}$ and thus not a saddle point in the Li migration pathway between Sn_{24} cages). The migration barriers for Li movement through the hexagonal face in Si_{46} and Ge_{46} are 0.35 and 0.09 eV, respectively. Previous estimates have suggested that ionic migration barriers should be, at most, in the range of 0.525−0.65 eV for materials to be effective as battery electrodes.[49] The NEB results for Li movement between adjacent Tt_{20} and Tt_{24} cages through the interconnected pentagonal face are presented in Figure 3b, with a schematic of the Li pathway for Si_{46} in the inset (Figure S2 shows the analogous schematics for Ge_{46} and Sn_{46}). Ge_{46} shows a very shallow local minimum at reaction coordinate 1, an indication of the flat energy landscape inside the Ge_{20} cage for Li. The energy barriers for Li moving through the

DOI: 10.1021/acs.jpcc.9b06424
J. Phys. Chem. C 2019, 123, 22812−22822

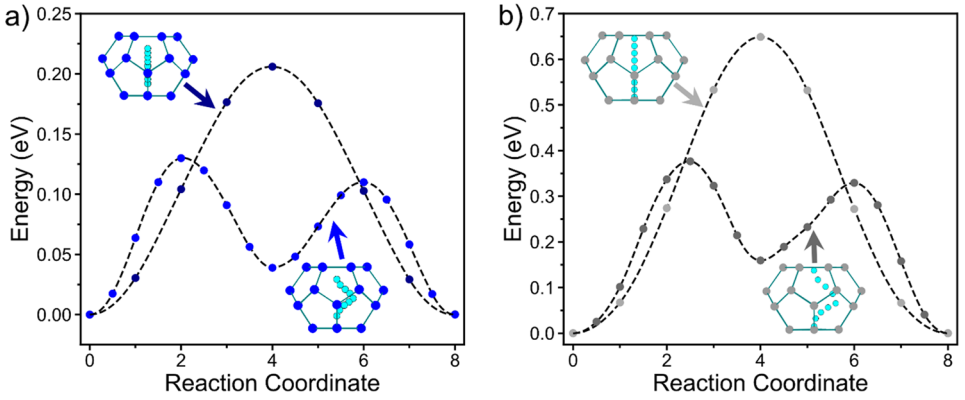

Figure 4. NEB-calculated minimum energy paths for Tt_{24} intracage migration of Li (cyan) in (a) Ge_{46} and (b) Sn_{46}. Pathway is between Off Hex positions through the center of the cage or along the side of the cage.

pentagonal face are 2.05, 1.28, and 0.54 eV for Tt = Si, Ge, and Sn, respectively. Previously, calculations performed on type II Si clathrates showed that the barrier for Li and Na migration through a pentagonal face is much higher than that through a hexagonal face.[18,50] This is consistent with our findings in type I clathrates, despite the slightly different structures between type I and II clathrates.

The calculated results also indicate that Li intercage diffusion causes distortion of the Tt atoms bonded within the faces. When Li moves through the hexagonal face, the Tt atoms expand outward away from the Li as it passes through the center. A similar result is observed when Li moves through the pentagonal face, but the atoms are moved more significantly away from their initial positions due to the smaller initial area of the pentagon. This is illustrated in Figure 3c, which shows the increase in the area of the face (as a percentage of the initial area) at the highest energy image for Li migration through the hexagonal and pentagonal faces. There is more expansion of the hexagonal face for Si_{46} compared to Ge_{46} (5.9% vs 2.6%), demonstrating that the amount of expansion is related to the height of the migration barrier. The lower area expansion and transition state energy for Ge_{46} suggests that the larger starting size of the hexagon allows for Li transport with less structural perturbation, leading to a lower energy barrier. In contrast, the expansion of the pentagonal face is much higher, reaching almost 30% for Si. The higher energy barriers for Li migration through the pentagonal face can be rationalized by the much larger displacement of the surrounding Tt atoms and shorter Tt−Li lengths during migration. The Tt−Li bond lengths are presented in Table S2, and a schematic of the initial and transition states is shown in Figure S3. These data show that the shorter Tt−Li bond lengths at the transition state also correlate with the higher transition state energy. As the pentagon/hexagon expands to move away from the Li, the distortion of the surrounding framework from the tetrahedral configuration will also raise the energy. The saddle point will be pinned by these two competing mechanisms. From these results we see that the energy barrier decreases significantly when increasing the size of the framework atom for both types of intercage Li migration pathways. This can be explained by the longer Li−Tt bonds at the transition state, less structural perturbation, and the higher propensity for Ge and Sn to accommodate framework distortions away from the ideal tetrahedral structure. The results are similar to those found in another study that calculated the migration barriers for Li in diamond cubic Si, Ge and Sn, where the migration barrier was also found to decrease as the Tt atom size increased.[51]

For the Ge and Sn frameworks, the most favorable position for Li insertion was found to be close to the hexagonal face (position 3 in Figure 2), far from the cage center position, which suggests that transport within a Tt_{24} cage should also be considered. Si_{46} is not included because the lowest energy position, the Off Pent position, is closer to the cage center. Figure 4a and 4b shows the NEB calculations for Li movement between two Off Hex positions in Ge_{46} and Sn_{46} via two pathways: through the center or along the cage side. The lower energy pathway involved Li migrating along the side of the cage to the local minimum position at the Off Pent site (position 4 in Figure 2) and then moving to the other Off Hex position on the other side of the Tt_{24} cage. The highest energy along this pathway was 0.13 eV for Ge and 0.37 eV for Sn. Movement through the cage center resulted in higher energy barriers (0.2 and 0.65 eV for Ge and Sn, respectively), demonstrating that Li prefers to stay near the cage side. In general, Li in the lower energy (i.e., off-centered) positions inside the Tt_{24} cage have a Tt−Li distance of around 2.8−3.0 Å (Table S1). When Li is at the center of the Tt_{24} cage in Ge_{46} and Sn_{46} clathrates, the Li−Tt distance increases to 3.60 and 4.17 Å, respectively. The latter bond length is much longer than the lower energy Li−Tt distances, which results in a higher energy barrier for intracage movement of Li within Sn_{46} through this pathway.

Previously, calculations by Tse et al. showed that Li diffusion between Si_{20} cages in the type II Si clathrate structure was affected by the presence of nearby Ba guest atoms.[18] If Ba was in an adjacent cage (which would be a Si_{28} cage in type II clathrates), the lower energy pathway for Li migration between Si_{20} cages was to break a Si−Si bond rather than going through the center of the pentagonal face. To investigate the possibility of this type of cooperative Li migration in the type I clathrates, the NEB calculation for Li migration between the Si_{20} and the Si_{24} cages was performed in Si_{46} with all Si_{24} cages filled with Li in the Off Pent positions (i.e., Li_6Si_{46}). The results (Figure 5a) show that when Li occupies the other Si_{24} cages, the migrating Li will break a Si−Si bond instead of migrating through the center of the pentagonal face, since the former process is accompanied by a much lower energy barrier (0.77 vs 2.0 eV). Figure 5b and 5c shows crystal models of one Si_{20} cage and two Si_{24} cages at reaction coordinate 0 and at reaction coordinate 4 (the transition state). The Si atoms in black indicate the three pentagons that share the bond that becomes broken in the

DOI: 10.1021/acs.jpcc.9b06424
J. Phys. Chem. C 2019, 123, 22812−22822

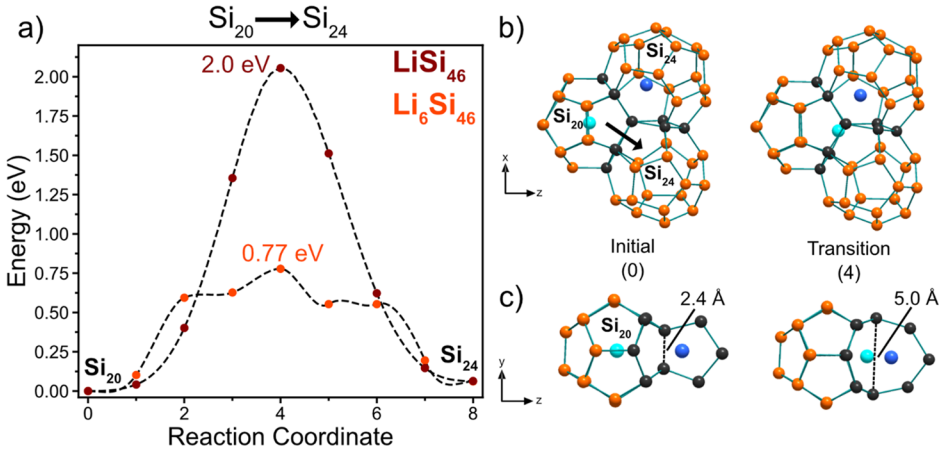

Figure 5. (a) NEB-calculated minimum energy paths for Li migrating from the Si_{20} cage to the Si_{24} cage with and without the adjacent Si_{24} cages filled with Li. (b) Crystal models of the intersection of two Si_{24} cages and one Si_{20} of the initial positions and the transition state positions for the minimum energy path in Li_6Si_{46}. Si atoms are orange, cyan atom is the mobile Li, and blue atom is Li in the adjacent Si_{24} cage. Si atoms in black are from the three pentagons that share the bond which is broken in the transition state. (c) Crystal model viewed down the *x* axis relative to b showing the Si−Si bond that is broken (dashed line).

transition state. The Si−Si bond originally has a bond length of 2.4 Å (Figure 5c); at the transition state, the Li atom (cyan) moves between the Si atoms and the Si distance increases to 5.0 Å, demonstrating that the Si−Si bond is replaced by Li−Si interactions. During Li migration from Si_{20} to Si_{24}, the Li occupying the adjacent Si_{24} cage (blue atom) moves 1.13 Å closer to the broken bond from its original position. The possibility for two Li atoms to stabilize the transition state is similar to results by Zhao et al., showing that as more Li surround the Si atoms during lithiation of diamond-structured Si it becomes more favorable to break the Si−Si bonds in favor of Li−Si bonds.[52] When repeating the calculation first reported by Tse et al.[18] for the migration of Li between Si_{20} cages in type II clathrate $LiBa_8Si_{136}$ (Figure S4), we found that during the transition the Ba atom moves 0.57 Å toward the broken Si−Si bond as well. This NEB pathway is visualized in Movies S1 and S2. These results suggest that cooperative motion between electroactive ions or guest atoms can result in a unique diffusion mechanism for accessing the Tt_{20} cages of clathrates, namely, by breaking and reforming a Tt bond.

The overall Li diffusion pathways in the type I clathrate frameworks can thus be described as follows. For Li in empty Si_{46}, the diffusion will be dominated by Li hopping between Si_{24} cages via hexagonal faces with a migration barrier of 0.35 eV. The high energy barrier (2.05 eV) for Li diffusion through pentagonal faces means that accessing the Si_{20} cage is unlikely in the dilute Li regime. If Li is already present in the other Si_{24} cages, the Si_{20} cages could be accessible to Li through a cooperative migration mechanism that involves Si bond breaking and results in a lower migration barrier of 0.77 eV. The Si_{24} cages will be preferentially occupied, and 1D diffusion can occur through the 3 perpendicular channels of Si_{24} cages connected by hexagonal faces. Ge_{46} shares a similar trend as Si_{46}, where intercage migration through the hexagonal face has the lowest energy barrier of 0.09 eV. However, intracage migration in the Ge_{24} cage has a higher energy barrier of 0.13 eV. The 1.28 eV barrier for intercage migration through the pentagonal face to the Ge_{20} cage will restrict access in the dilute Li regime. For Sn_{46}, the cage size becomes large enough that intracage migration in Sn_{46} is the major limiting factor with a migration barrier of 0.37 eV. Li occupation of the Sn_{20} cage is feasible in this case as well, with a migration barrier of 0.54 eV through the pentagonal face.

In summary, the Li diffusion in empty type I clathrates is predicted to be determined by movement between Tt_{24} cages via the hexagonal faces. As the cage size increases from Si_{46} to Sn_{46}, Li prefers to be closer to the side of the cage and intracage diffusion begins to be a more important factor for the migration barriers. Ge_{46}, with the lowest barrier of 0.13 eV, has a cage size that minimizes the intercage and intracage migration barriers, resulting in a flat energy landscape with regard to the possible Li positions. When the cage is smaller (e.g., Si_{46}), intercage transport via the hexagonal face is limiting, and when the cage is larger (e.g., Sn_{46}), intracage transport is limiting.

3.4. Na Positions and Migration Pathways in Empty Type I Clathrates. To find the most favorable Na positions in the empty type I clathrate structure, a treatment similar to the one used to study Li diffusion was applied by placing the Na in four positions: (1) Tt_{24} center, (2) Tt_{20} center, (3) Off Hex, and (4) Off Pent. The ΔG_r for Tt_{46} with one Na is presented in Figure 6, with the associated crystal structures showing the position of Na after relaxation. Table S3 shows the Tt−Na bond lengths and lattice parameters of the relaxed structures.

For $NaSi_{46}$, Na occupation is favorable inside both the Si_{20} and the Si_{24} cages as shown by the negative ΔG_r values calculated for the relaxed positions. When the initial positions are off-center of the hexagonal or pentagonal faces in the Si_{24} cage, the Na moves to the center after relaxation. Different from the Li case, Na prefers the center position of both Si_{24} and Si_{20} cages. This is consistent with well-documented experimental evidence that shows Na occupation in both cage center positions of Na_8Si_{46} with low thermal displacement parameters,[45,53,54] indicating low disorder on the Na site. For $NaGe_{46}$ and $NaSn_{46}$, the calculations indicate that it is also favorable for Na to occupy both cages, as shown by the negative ΔG_r values. Similar to the case for Si_{46}, Na prefers the center of the Ge_{24} cage when relaxed from the initial Off Hex and Off Pent positions. The Off Pent site is the most favorable position for Na inside the Sn_{24} cage. This position is similar to the off-centered positions reported for K and Ba in Sn_{24} cages, where splitting in the anisotropic thermal displacement

DOI: 10.1021/acs.jpcc.9b06424
J. Phys. Chem. C 2019, 123, 22812−22822

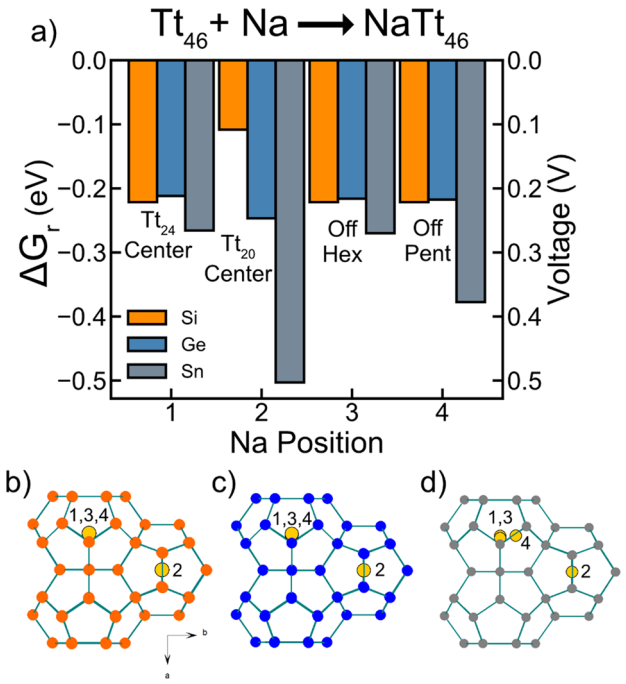

Figure 6. (a) Gibbs free energy change of reaction (ΔG_r) and voltage vs Na/Na^+ for the reaction Tt_{46} + Na → $NaTt_{46}$, where Tt = Si, Ge, and Sn, for each of the 4 Na positions. Schematic of two Tt_{24} cages and one Tt_{20} cage for (b) Si_{46}, (c) Ge_{46}, and (d) Sn_{46} showing the 4 Na positions after relaxation viewed down the [100] direction. Na = yellow, Si = orange, Ge = blue, Sn = gray.

parameters shows disorder in the directions parallel to the hexagonal faces.[43,55] Despite the energetic favorability for occupation of Na in Ge_{46} and Sn_{46}, to our knowledge, no Na-containing, type I Ge and Sn clathrates have been synthesized, although Na-containing, type II Ge clathrates have been prepared via thermal decomposition of Na_4Ge_4.[10] The negative ΔG_r values for all of the investigated Na positions in the Tt_{46} clathrates also suggest that the electrochemical sodiation of all compositions is energetically favorable if the kinetics allow it.

Next, the NEB calculations for Na migration between Tt_{24} cages through the hexagonal face and then from the Tt_{20} cage to the Tt_{24} cage are presented in Figure 7a and 7b. The migration barriers for Na through the hexagonal face (Figure 7a) for Si, Ge, and Sn are 2.42, 1.48, and 0.45 eV, respectively. Na migration in Sn_{46} is slightly different from that in Si_{46} and Ge_{46} as the initial (i.e., lowest energy position) is the Off Pent position (Na Position 4 in Figure 6d); a crystal model schematic of the NEB pathway is shown in the inset of Figure 7a. The local minimum at reaction coordinate 2 is an intracage transition from an Off Pent to Off Hex position within the Sn_{24} cage. Similar to the case of Li migration, Na is found to move through the center of the hexagonal face and forces the six Tt atoms to move away from the Na atom, resulting in an increase in the area of the hexagon of 15.6%, 15.1%, and 9.6% for Si, Ge, and Sn, respectively (Figure 7c). Compared to Li migration, the area expansion of the hexagonal face and the migration energies for Na migration are higher. This can be attributed to the larger size of Na and longer Tt−Na interaction distances, which is evident from the preference of Na for the Tt_{24} cage center. The Tt−Na distances for the hexagonal transition states are provided in Table S4. Initially,

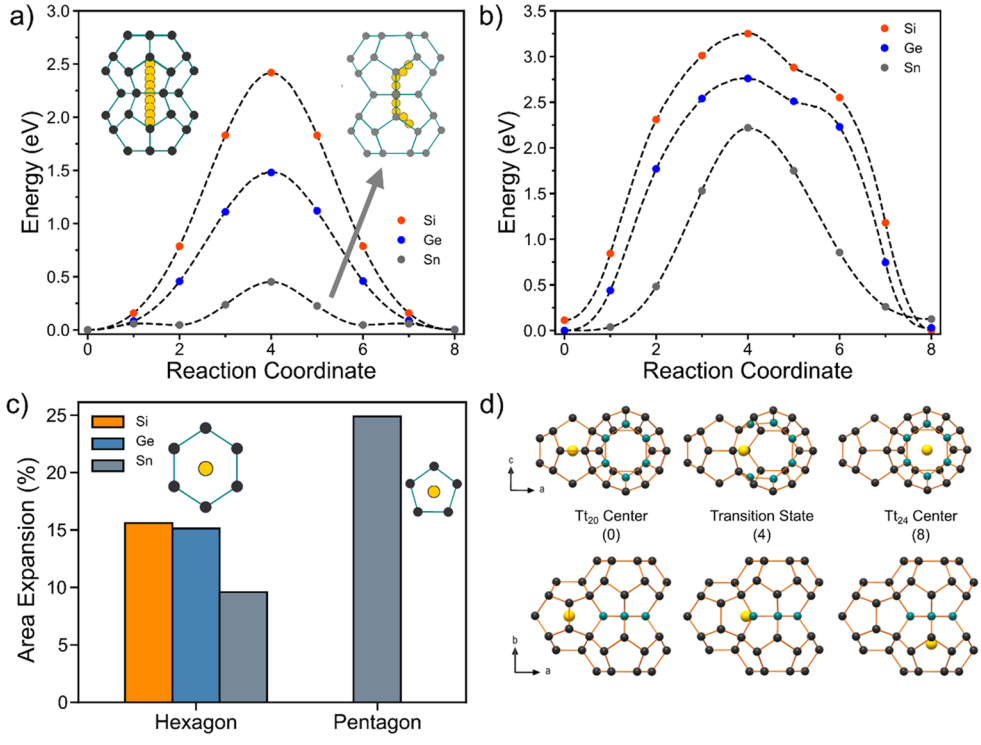

Figure 7. (a) NEB-calculated minimum energy paths for Na (yellow) migration in Si_{46} and Ge_{46} (black) and Sn_{46} (gray) through the hexagonal face. (b) NEB-calculated minimum energy paths for Na migration between the Tt_{20} and the Tt_{24} cages for Tt_{46} through a pentagonal face. (c) Percentage of areal expansion of the hexagonal and pentagonal face in the type I clathrate structure at the highest energy position (reaction coordinate 4) in a and b relative to the starting size of the hexagon/pentagon. (d) Crystal models of $NaSi_{46}$ and $NaGe_{46}$ at the 0, 4, and 8 reaction coordinate of b viewed down the *b* and *c* axes. Teal atoms indicate those in the hexagonal face.

DOI: 10.1021/acs.jpcc.9b06424
J. Phys. Chem. C 2019, 123, 22812−22822

the Na−Tt distances are 3.44−3.65 Å. At the transition state, the Na−Tt bond lengths decrease dramatically (i.e., 2.52 Å for the Si_{46} case), which correlates with the high migration barrier.

Figure 7b shows the NEB results for Na migration between Tt_{20} and Tt_{24} cages. The migration barriers are 3.25, 2.76, and 2.22 eV for Si, Ge and Sn, respectively. For Si_{46} and Ge_{46}, when migrating from a Tt_{20} to Tt_{24} cage, Na will preferentially break a Tt bond instead of passing through the center of the pentagonal face. The increased asymmetry in the NEB minimum energy path in Figure 7b is a result of this Tt bond breaking. The reaction path is illustrated in Figure 7d, showing the crystal structures of reaction coordinate 0, 4, and 8 in the NEB calculation from two viewing directions. This $NaSi_{46}$ NEB pathway is also visualized in Movies S3 and S4. At the transition state, the Tt bond is broken as the Na migrates between the two Tt atoms. This mechanism is similar to that which was previously described for the Li case in Si_{46} (Figure 5). However, no other guest or Na atom is needed in an adjacent Tt_{24} cage to allow the system to converge to this minimum energy path. This could be explained by considering the extremely unfavorable transition of Na moving through a Tt pentagonal face, which would likely cause large perturbation to the position of the Tt atoms and result in very short Na−Tt distances. This bond-breaking pathway is then favored by significantly perturbing two Tt atoms and stabilizing the broken bonds with the Na atom. For Sn_{46}, the minimum energy path does not converge to this Na migration pathway, and instead, the Na passes through the pentagonal center. This is possibly because the Sn pentagon is large enough to sustain framework distortions while maintaining longer Sn−Na distances during the transition state. Since Na migration from Si_{20} cages is relevant for the thermal desodiation of Na_xSi_{136} under vacuum, a synthetic approach to access guest-free type II clathrates,[29,30,50,56] a calculation for Na diffusion from a Si_{20} to a Si_{28} cage was also performed to see if this bond-breaking phenomenon occurs. Figure S5 shows the NEB minimum energy path and crystal structures of this path; the results show that this Na migration pathway in the type II clathrate does indeed result in the breaking of a Si−Si bond but with a lower activation energy of 2.48 eV (vs 3.25 eV in type I Si_{46} clathrate). The NEB pathway for $NaSi_{136}$ is visualized in Movies S5 and S6. The implications and significance of these results will be described in section 4.2.

The overall diffusion pathways for Na in Tt_{46} frameworks can now be summarized. The lowest energy migration paths involve transport through the hexagonal face between Tt_{24} cages through the 1D channels. Accessing the Tt_{20} cages involves a higher energy transition state via a bond-breaking mechanism for Si_{46} and Ge_{46}. For room-temperature diffusion, the energy barriers are too high in Si_{46} (2.42 eV) and Ge_{46} (1.48 eV) for any significant Na ionic mobility.[49] On the other hand, for Sn_{46}, the lower barrier of 0.45 eV could allow Na hopping between Sn_{24} cages. Overall, when compared to Li, Na has much lower mobility in guest-free, type I clathrate frameworks due to its larger atomic size and preference for longer bond distances to the Tt atoms.

A similar analysis for Mg guest atoms was also calculated, and the Gibbs free energy change of reaction values is shown in Figure S6. The ΔG_r for all four positions were positive, with values above 0.5 eV for the three Tt compositions investigated, suggesting that these reactions are unfavorable. This is consistent with no known reports of clathrates containing Mg guest atoms.

4. DISCUSSION

4.1. Comparison of Li Migration in Clathrates vs Diamond Structure and Other Open Frameworks.

The Li environment in guest-free, type I clathrates is distinctly unique to that in diamond-structured analogs. The tetrahedral "cavities" that are known to be the stable Li positions in the diamond structure are much smaller than the cavities in the clathrate cages and are more densely packed.[51,57] The Li tetrahedral position allows for symmetric interaction with the four surrounding Tt atoms, resulting in a minimum in the energy landscape for the Li interstitial. Transport between these tetrahedral interstitial positions is through a hexagonal-like ring of Tt atoms which have Li migration barriers previously calculated as 0.62, 0.44, and 0.39 eV for Si, Ge, and Sn, respectively.[51]

For the clathrates, Li can also traverse through a hexagonal ring between Tt_{24} cages but with lower energy barriers of 0.35 and 0.09 eV for Si_{46} and Ge_{46} (Figure 3a), respectively. This difference can be attributed to the destabilization of the Li site energies inside the Tt_{24} cages. The Tt_{24} cages are too large for favorable Li−Tt interactions when Li is in the cage center, which results in Li preferring to be close to the cage side near one of the hexagonal or pentagonal faces. This site preference removes the favorable Li−Tt symmetric interaction from all sides (such as that in the tetrahedral position in the diamond structure) and frustrates the Li energy landscape when it occupies the Tt_{24} cage. This results in multiple Li positions with similar energies. In other words, the open framework structure of the clathrates smooths out the energy landscape for a Li intercalant by removing highly symmetric positions that act as low-energy minima. This has the effect of decreasing the relative difference between Li resting sites and the transition state, leading to lower energy barriers for Li migration through the hexagonal face (0.35 and 0.09 eV for Si_{46} and Ge_{46}, respectively) compared to those seen in the diamond structures (0.62 and 0.44 eV for Si and Ge, respectively).

Among the Tt_{46} clathrates investigated here, the Ge_{46} clathrate displays the lowest Li migration energy barriers. The energy difference among the different Li positions in the Tt_{24} cage is low (~0.2 eV), and the hexagonal face is large enough to enable facile Li migration between Tt_{24} cages (0.09 eV barrier). This balance between the size of hexagonal face and the Tt_{24} cage leads to the lowest Li migration barrier among the compositions investigated here. This concept is summarized in Figure 8, where two adjoining Tt_{24} cages are

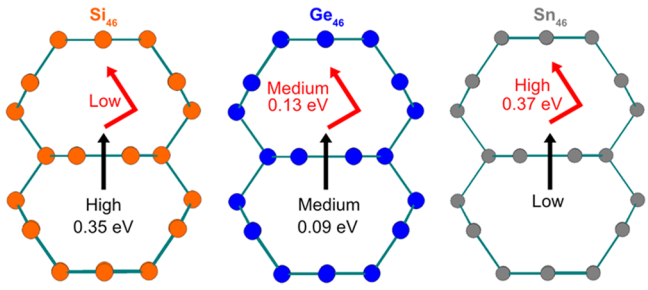

Figure 8. Scheme summarizing the relative energy barriers for Li intracage (red arrows) and intercage (black arrows) migration through two adjoining Tt_{24} cages (shown in cross-section) connected by a hexagonal face. As the cage size increases, the intracage barrier increases while the intercage barrier decreases.

DOI: 10.1021/acs.jpcc.9b06424
J. Phys. Chem. C 2019, 123, 22812−22822

labeled with the relative intracage (red arrows) and intercage (black arrows) migration barriers. When the cage size is smaller, as is the case of Si_{46}, the highest energy position is the transition state at the center of the hexagonal face, which leads to a higher energy barrier for intercage diffusion (0.35 eV). When the cage is larger, as in the case of Sn_{46}, unfavorable Tt−Li interactions at the cage center lead to a larger relative energy difference among the possible Li sites and a higher migration barrier for intracage diffusion (0.37 eV). Ge_{46} is the intermediate case between these two extremes, with relatively low barriers for both intracage and intercage migration. These results suggest that the size of the cage (and by extension, the channels through which the guest atoms diffuse) are the primary factors for determining the migration barriers and hence could potentially be tuned by creating alloys of these Tt_{46} compounds.

Recent theoretical studies investigating a new Si polymorph (Si_{24})[31] with similar structural features as clathrates reported a low migration barrier of 0.14 eV for Li hopping and high room-temperature conductivity from ab initio molecular dynamics calculations.[46,58] The Si_{24} structure is composed of channels of hexagonal-like rings in which Li is predicated to migrate, similar to the results found here. The calculated migration barriers for type I clathrates and Si_{24} are similar to those of Li-ion superionic conductors, which have activation barriers of around 0.2−0.3 eV,[59] suggesting that Li migration would be facile. Hence, open, covalently bonded frameworks of Tt atoms appear to have promising ionic mobility for Li if there are no guest atoms present.

4.2. Comparison of Li and Na Migration in Clathrates.

Compared to Li, Na intercalation appears to be severely limited by the fact that it is relatively difficult to squeeze the larger Na atom size through the hexagons and pentagons connecting adjacent clathrate cages. Except in the case of Sn_{46}, the calculated Na migration barriers suggest that the diffusion of Na between cages would be limited. This is well supported by the experimental evidence that Na evaporation from Na_xSi_{136} occurs in the temperature range of 370−450 °C under vacuum,[28,30,45,56] indicating that the migration barriers for Na diffusion from the bulk to the surface are much higher than those that would enable significant room-temperature diffusion. The type I clathrate Na_8Si_{46} does not exhibit Na loss via evaporation under similar conditions as Na_xSi_{136}, suggesting that Na migration in type I clathrates is even more limited. Effectively, the diffusion channels are too narrow to allow for facile Na migration. This is in contrast with Li, which has close to the ideal size (Tt−Li length of 2.8−3.0 Å) for migrating through hexagonal faces composed of Tt atoms. Only in Sn_{46}, which has larger sized hexagons compared to Si_{46} and Ge_{46}, can the Na atom diffuse with a migration barrier of 0.45 eV, pointing to the possibility of Na intercalation in guest-free Sn clathrates.

The unique bond-breaking migration mechanism for Na migration to and from the Tt_{20} cage highlights the highly unfavorable pathway of intercalants squeezing through the Tt pentagons. Unlike Li migration, the pentagonal transition state in the case of Na migration is obtained without cooperative motion and is likely due to the very high energy of the pentagonal pathway in comparison to breaking a Tt−Tt bond. This mechanism is particularly interesting for explaining the Na diffusion in type II Si clathrates, where it has been suggested that Na moves from the Si_{20} to the Si_{28} cages through a pentagonal face.[50] As seen in Figure S6, when migrating from the Si_{20} to the Si_{28} cages, Na will cleave and reform a Si−Si bond instead of moving through the center of the pentagon face, which has an energy barrier of 2.48 eV. These results could help explain the diffusion mechanism of Na evaporation from type II Si clathrates during thermal treatment under vacuum.

5. CONCLUSIONS

In summary, DFT calculations were used to evaluate the preferred insertion positions and migration pathways for Li and Na in guest-free, type I clathrate frameworks composed of Si, Ge, and Sn. Because of the size mismatch between Li and the Tt_{24} cages, Li prefers a more off-center position inside the Tt_{24} cage as the size of the cage increases in Si to Sn clathrates. In the smaller Tt_{20} cages, it is more energetically favorable for Li to be closer to the center position of the cage. The diffusion paths for Li in the structures is determined by the connectivity of the cages via hexagonal faces. The barrier for Li to migrate through a hexagonal face is much lower (0.35 eV for Si_{46}) than diffusing through a pentagonal one (2.05 eV), meaning that Li hopping between Tt_{24} cages will dominate the Li migration. Li insertion into the Tt_{20} cage would be kinetically restricted due to the high migration barrier in the dilute regime. However, we find that a lower energy pathway characteristic of cooperative migration (barrier of 0.77 eV) is possible where the Li breaks a Si−Si bond at the transition state if Li atoms are present in adjacent cages. The cage size for Ge_{46} results in a flat energy landscape for the Li positions, leading to a lower barrier of 0.13 eV for migration, which is comparable to barriers in current superionic conductors. The low migration barriers for Li in the Tt_{46} structures suggest the possibility of Li insertion and thus possible applications for Li-ion batteries.

In contrast to the low migration barriers for Li there are high barriers for Na migration (2.5 eV for Si_{46}) through the hexagonal face between Tt_{24} cages. This is attributed to the larger size of the Na atom and its longer Na−Tt bond distance (~3.5 Å) compared to the Li−Tt distances (~3.0 Å). Movement of Na to the Tt_{20} cage results in a similar bond-breaking mechanism as seen in the Li case but without the need for cooperative motion of another metal atom in the adjacent cage. This points to the unfavorability of Na moving through a Tt pentagon and the general sluggishness of Na migration. In the case of Sn_{46}, the migration barrier through the hexagon is 0.45 eV, suggesting the feasibility of Na insertion into Sn clathrates. Although the ion mobility is high in some cases, the difficulty to synthesize guest-free, type I clathrates currently preclude experimental support of these results. However, the insights presented here are informative for understanding the synthesis of guest-free materials via chemical deintercalation routes and may be helpful for the design of novel synthetic methods for these open framework materials.

■ ASSOCIATED CONTENT

Supporting Information

The Supporting Information is available free of charge on the ACS Publications website at DOI: 10.1021/acs.jpcc.9b06424.

Movie of the NEB pathway of $LiBa_8Si_{136}$ showing the Si−Si bond breaking and reforming (AVI)

Movie of the NEB pathway of $LiBa_8Si_{136}$ from another view showing Li diffusion between Si_{20} cages (AVI)

DOI: 10.1021/acs.jpcc.9b06424
J. Phys. Chem. C 2019, 123, 22812−22822

Movie of the NEB pathway of $NaSi_{46}$ for Na diffusion from Si_{20} to Si_{24} showing the Si−Si bond breaking and reforming (AVI)

Movie of the NEB pathway of $NaSi_{46}$ for Na diffusion from Si_{20} to Si_{24} showing Na migration between Si_{20} and Si_{24} cages (AVI)

Movie of the NEB pathway of $NaSi_{136}$ for Na diffusion from Si_{20} to Si_{28} showing the Si−Si bond breaking and reforming (AVI)

Movie of the NEB pathway of $NaSi_{136}$ for Na diffusion from Si_{20} to Si_{28} showing Na migration between Si_{20} and Si_{28} cages (AVI)

Calculated shortest Li−Tt distances and lattice parameters for the Tt_{46} structures presented in Figure 2; calculated Li−Tt bond lengths for the initial and transition states, and energy of the highest energy image from NEB results in Figure 3a and 3b; calculated shortest Na−Tt distances and lattice parameters for the Tt_{46} structures presented in Figure 6; calculated Na−Tt bond lengths for the initial and transition states, and energy of the highest energy image from the NEB results in Figure 7a and 7b; crystal model schematic of Sn_{46} showing the energy and position of the Off-Pent position in the Sn_{20} cage; crystal models schematics of NEB pathways for pentagonal migration in Ge_{46} and Sn_{46} of Li shown in Figure 3b; crystal model structures of a single Tt_{24} cage showing examples of the initial and transition states for Na or Li during migration; NEB minimum energy path for $LiBa_8Si_{136}$ (type II Si clathrate) for Li migration between two Si_{20} cages; Gibbs free energy change of reaction (ΔG_r) and voltage vs Mg/Mg^+ when Mg was placed in each of the 4 positions for the reaction $Tt_{46} + Mg \rightarrow MgTt_{46}$; crystal model schematic of NEB pathway for hexagonal migration of Na (Figure 7a) in Sn_{46}; NEB minimum energy path for the Na migration in $NaSi_{136}$ (type II Si clathrate) between the Si_{28} and the Si_{20} cages; theoretical capacities of Si_{46}, Ge_{46}, Sn_{46}, Si_{24}, LTO, and graphite (PDF)

AUTHOR INFORMATION

Corresponding Authors

*E-mail: xihong.peng@asu.edu.

*E-mail: candace.chan@asu.edu.

ORCID

Candace K. Chan: 0000-0003-4329-4865

Author Contributions

A.D. and X.P. performed the DFT calculations. C.K.C. conceived the project and assisted with the analysis. All authors contributed to the writing and have given approval to the final version of the manuscript.

Notes

The authors declare no competing financial interest.

ACKNOWLEDGMENTS

This work was supported by funding from NSF DMR-1710017. A.D. acknowledges support from ASU Fulton Schools of Engineering Dean's Fellowship. The authors greatly acknowledge the use of computational facilities (Agave and Saguaro Clusters) within the Advanced Computing Center at Arizona State University.

REFERENCES

(1) Griffith, K. J.; Wiaderek, K. M.; Cibin, G.; Marbella, L. E.; Grey, C. P. Niobium Tungsten Oxides for High-Rate Lithium-Ion Energy Storage. *Nature* **2018**, *559*, 556−563.

(2) Di Stefano, D.; Miglio, A.; Robeyns, K.; Filinchuk, Y.; Lechartier, M.; Senyshyn, A.; Ishida, H.; Spannenberger, S.; Roling, B.; Kato, Y.; et al. Superionic Diffusion through Frustrated Energy Landscape. *Chem* **2019**. DOI: 10.1016/j.chempr.2019.07.001

(3) Kawaji, H.; Horie, H.; Yamanaka, S.; Ishikawa, M. Superconductivity in the Silicon Clathrate Compound $(Na, Ba)_xSi_{46}$. *Phys. Rev. Lett.* **1995**, *74*, 1427−1429.

(4) Reny, E.; San-Miguel, A.; Guyot, Y.; Masenelli, B.; Mélinon, P.; Saviot, L.; Yamanaka, S.; Champagnon, B.; Cros, C.; Pouchard, M.; et al. Vibrational Modes in Silicon Clathrate Compounds: A Key to Understanding Superconductivity. *Phys. Rev. B: Condens. Matter Mater. Phys.* **2002**, *66*, 014532.

(5) Connétable, D.; Timoshevskii, V.; Masenelli, B.; Beille, J.; Marcus, J.; Barbara, B.; Saitta, A. M.; Rignanese, G. M.; Mélinon, P.; Yamanaka, S.; et al. Superconductivity in Doped Sp3 Semiconductors: The Case of the Clathrates. *Phys. Rev. Lett.* **2003**, *91*, 247001.

(6) Fukuoka, H.; Kiyoto, J.; Yamanaka, S. Superconductivity and Crystal Structure of the Solid Solutions of $Ba_{8-\delta}Si_{46-x}Ge_x$ ($0 \leq x \leq 23$) with Type I Clathrate Structure. *J. Solid State Chem.* **2003**, *175*, 237−244.

(7) Bryan, J. D.; Srdanov, V. I.; Stucky, G. D.; Schmidt, D. Superconductivity in Germanium Clathrate $Ba_8Ga_{16}Ge_{30}$. *Phys. Rev. B: Condens. Matter Mater. Phys.* **1999**, *60*, 3064−3067.

(8) Neiner, D.; Okamoto, N. L.; Condron, C. L.; Ramasse, Q. M.; Yu, P.; Browning, N. D.; Kauzlarich, S. M. Hydrogen Encapsulation in a Silicon Clathrate Type I Structure: $Na_{5.5}(H_2)_{2.15}Si_{46}$: Synthesis and Characterization. *J. Am. Chem. Soc.* **2007**, *129*, 13857−13862.

(9) Neiner, D.; Okamoto, N. L.; Yu, P.; Leonard, S.; Condron, C. L.; Toney, M. F.; Ramasse, Q. M.; Browning, N. D.; Kauzlarich, S. M. Synthesis and Characterization of $K_{8-x}(H_2)_ySi_{46}$. *Inorg. Chem.* **2010**, *49*, 815−822.

(10) Baranowski, L. L.; Krishna, L.; Martinez, A. D.; Raharjo, T.; Stevanović, V.; Tamboli, A. C.; Toberer, E. S. Synthesis and Optical Band Gaps of Alloyed Si−Ge Type II Clathrates. *J. Mater. Chem. C* **2014**, *2*, 3231.

(11) Blake, N. P.; Mollnitz, L.; Kresse, G.; Metiu, H. Why Clathrates Are Good Thermoelectrics: A Theoretical Study of $Sr_8Ga_{16}Ge_{30}$. *J. Chem. Phys.* **1999**, *111*, 3133−3144.

(12) Nolas, G. S.; Slack, G. A.; Schujman, S. B. Chapter 6 Semiconductor Clathrates: A Phonon Glass Electron Crystal Material with Potential for Thermoelectric Applications. *Semicond. Semimetals* **2001**, *69*, 255−300.

(13) Tsujii, N.; Roudebush, J. H.; Zevalkink, A.; Cox-Uvarov, C. A.; Jeffery Snyder, G.; Kauzlarich, S. M. Phase Stability and Chemical Composition Dependence of the Thermoelectric Properties of the Type-I Clathrate $Ba_8Al_xSi_{46-x}$ ($8 \leq x \leq 15$). *J. Solid State Chem.* **2011**, *184*, 1293−1303.

(14) Saramat, A.; Svensson, G.; Palmqvist, A. E. C.; Stiewe, C.; Mueller, E.; Platzek, D.; Williams, S. G. K.; Rowe, D. M.; Bryan, J. D.; Stucky, G. D. Large Thermoelectric Figure of Merit at High Temperature in Czochralski-Grown Clathrate $Ba_8Ga_{16}Ge_{30}$. *J. Appl. Phys.* **2006**, *99*, 023708.

(15) Nolas, G. S.; Cohn, J. L.; Slack, G. A.; Schujman, S. B. Semiconducting Ge Clathrates: Promising Candidates for Thermoelectric Applications. *Appl. Phys. Lett.* **1998**, *73*, 178−180.

(16) Uemura, T.; Akai, K.; Koga, K.; Tanaka, T.; Kurisu, H.; Yamamoto, S.; Kishimoto, K.; Koyanagi, T.; Matsuura, M. Electronic Structure and Thermoelectric Properties of Clathrate Compounds $Ba_8Al_xGe_{46-x}$. *J. Appl. Phys.* **2008**, *104*, 013702.

(17) Langer, T.; Dupke, S.; Trill, H.; Passerini, S.; Eckert, H.; Pöttgen, R.; Winter, M. Electrochemical Lithiation of Silicon Clathrate-II. *J. Electrochem. Soc.* **2012**, *159*, A1318−A1322.

(18) Yang, J.; Tse, J. S. Silicon Clathrates as Anode Materials for Lithium Ion Batteries? *J. Mater. Chem. A* **2013**, *1*, 7782.

(19) Wagner, N. A.; Raghavan, R.; Zhao, R.; Wei, Q.; Peng, X.; Chan, C. K. Electrochemical Cycling of Sodium-Filled Silicon Clathrate. *ChemElectroChem* **2014**, *1*, 347−353.
(20) Li, Y.; Raghavan, R.; Wagner, N. A.; Davidowski, S. K.; Baggetto, L.; Zhao, R.; Cheng, Q.; Yarger, J. L.; Veith, G. M.; Ellis-Terrell, C.; et al. Type I Clathrates as Novel Silicon Anodes: An Electrochemical and Structural Investigation. *Adv. Sci.* **2015**, *2*, 1500057.
(21) Peng, X.; Wei, Q.; Li, Y.; Chan, C. K. First-Principles Study of Lithiation of Type I Ba-Doped Silicon Clathrates. *J. Phys. Chem. C* **2015**, *119*, 28247−28257.
(22) Chan, K. S.; Miller, M. A.; Liang, W.; Ellis-Terrell, C.; Chan, C. K. First Principles and Experimental Studies of Empty Si46 as Anode Materials for Li-Ion Batteries. *J. Mater. Res.* **2016**, *31*, 3657−3665.
(23) Warrier, P.; Koh, C. A. Silicon Clathrates for Lithium Ion Batteries: A Perspective. *Appl. Phys. Rev.* **2016**, *3*, 040805.
(24) Bohme, B.; Bonatto Minella, C.; Thoss, F.; Lindemann, I.; Rosenburg, M.; Pistidda, C.; Møller, K. T.; Jensen, T. R.; Giebeler, L.; Baitinger, M.; Gutfleisch, O.; Ehrenberg, H.; Eckert, J.; Grin, Y.; Schultz, L.; et al. B1-Mobilstor: Materials for Sustainable Energy Storage Techniques - Lithium Containing Compounds for Hydrogen and Electrochemical Energy Storage. *Adv. Eng. Mater.* **2014**, *16*, 1189−1195.
(25) Zhao, R.; Bobev, S.; Krishna, L.; Yang, T.; Weller, J. M.; Jing, H.; Chan, C. K. Anodes for Lithium-Ion Batteries Based on Type I Silicon Clathrate $Ba_8Al_{16}Si_{30}$ - Role of Processing on Surface Properties and Electrochemical Behavior. *ACS Appl. Mater. Interfaces* **2017**, *9*, 41246−41257.
(26) Dopilka, A.; Zhao, R.; Weller, J. M.; Bobev, S.; Peng, X.; Chan, C. K. Experimental and Computational Study of the Lithiation of $Ba_8Al_yGe_{46-y}$ Based Type I Germanium Clathrates. *ACS Appl. Mater. Interfaces* **2018**, *10*, 37981−37993.
(27) Taylor, P. C. Exotic Forms of Silicon. *Phys. Today* **2016**, *69*, 34−39.
(28) Kasper, J. S.; Hagenmuller, P.; Pouchard, M.; Cros, C. Clathrate Structure of Silicon Na_8Si_{46} and Na_xSi_{136} ($x < 11$). *Science* **1965**, *150*, 1713−1714.
(29) Beekman, M.; Nolas, G. S. Synthesis and Thermal Conductivity of Type II Silicon Clathrates. *Phys. B* **2006**, *383*, 111−114.
(30) Krishna, L.; Baranowski, L. L.; Martinez, A. D.; Koh, C. A.; Taylor, P. C.; Tamboli, A. C.; Toberer, E. S. Efficient Route to Phase Selective Synthesis of Type II Silicon Clathrates with Low Sodium Occupancy. *CrystEngComm* **2014**, *16*, 3940−3949.
(31) Kim, D. Y.; Stefanoski, S.; Kurakevych, O. O.; Strobel, T. A. Synthesis of an Open-Framework Allotrope of Silicon. *Nat. Mater.* **2015**, *14*, 169−173.
(32) Nakano, H.; Ikuno, T. Soft Chemical Synthesis of Silicon Nanosheets and Their Applications. *Appl. Phys. Rev.* **2016**, *3*, 040803.
(33) Guloy, A. M.; Ramlau, R.; Tang, Z.; Schnelle, W.; Baitinger, M.; Grin, Y. A Guest-Free Germanium Clathrate. *Nature* **2006**, *443*, 320−323.
(34) Scherf, L. M.; Hattendorff, J.; Buchberger, I.; Geier, S.; Gasteiger, H. A.; Fässler, T. F. Electrochemical Synthesis of the Allotrope Allo-Ge and Investigations on Its Use as an Anode Material. *J. Mater. Chem. A* **2017**, *5*, 11179−11187.
(35) Cultrara, N. D.; Wang, Y.; Arguilla, M. Q.; Scudder, M. R.; Jiang, S.; Windl, W.; Bobev, S.; Goldberger, J. E. Synthesis of 1T, 2H, and 6R Germanane Polytypes. *Chem. Mater.* **2018**, *30*, 1335−1343.
(36) Kresse, G.; Furthmüller, J. Efficient Iterative Schemes for Ab Initio Total-Energy Calculations Using a Plane-Wave Basis Set. *Phys. Rev. B: Condens. Matter Mater. Phys.* **1996**, *54*, 11169−11186.
(37) Kresse, G.; Joubert, D. From Ultrasoft Pseudopotentials to the Projector Augmented-Wave Method. *Phys. Rev. B: Condens. Matter Mater. Phys.* **1999**, *59*, 1758−1775.
(38) Perdew, J. P.; Burke, K.; Ernzerhof, M. Generalized Gradient Approximation Made Simple. *Phys. Rev. Lett.* **1996**, *77*, 3865−3868.
(39) *Jmol: An Open-Source Java Viewer for Chemical Structures in 3D*; http://www.jmol.org/.
(40) Henkelman, G.; Uberuaga, B. P.; Jónsson, H. Climbing Image Nudged Elastic Band Method for Finding Saddle Points and Minimum Energy Paths. *J. Chem. Phys.* **2000**, *113*, 9901−9904.
(41) Bhattacharya, A.; Carbogno, C.; Böhme, B.; Baitinger, M.; Grin, Y.; Scheffler, M. Formation of Vacancies in Si- and Ge-Based Clathrates: Role of Electron Localization and Symmetry Breaking. *Phys. Rev. Lett.* **2017**, *118*, 1−5.
(42) Saito, S.; Oshiyama, A. Electronic Structure of Si_{46} and $Na_2Ba_6Si_{46}$. *Phys. Rev. B: Condens. Matter Mater. Phys.* **1995**, *51*, 2628−2631.
(43) Kaltzoglou, A.; Ponou, S.; Fässler, T. F. Synthesis and Crystal Structure of Mercury-Substituted Type-I Clathrates $A_8Hg_4Sn_{42}$ (A = K, Rb, Cs). *Eur. J. Inorg. Chem.* **2008**, *2008*, 538−542.
(44) Schnering, H. G. v.; Llanos, J.; Peters, K.; Baitinger, M.; Grin, Y.; Nesper, R. Refinement of the Crystal Structure of $K_8Ge_{44}\square_2$, an Intermetallic Clathrate I. *Z. Kristallogr. - New Cryst. Struct.* **2011**, *226*, 9−10.
(45) Ramachandran, G. K.; Dong, J.; Diefenbacher, J.; Gryko, J.; Marzke, R. F.; Sankey, O. F.; McMillan, P. F. Synthesis and X-Ray Characterization of Silicon Clathrates. *J. Solid State Chem.* **1999**, *145*, 716−730.
(46) Arrieta, U.; Katcho, N. A.; Arcelus, O.; Carrasco, J. First-Principles Study of Sodium Intercalation in Crystalline Na_xSi_{24} ($0 \leq x \leq 4$) as Anode Material for Na-Ion Batteries. *Sci. Rep.* **2017**, *7*, 5350.
(47) Kim, H.; Kim, D. J.; Seo, D. H.; Yeom, M. S.; Kang, K.; Kim, D. K.; Jung, Y. Ab Initio Study of the Sodium Intercalation and Intermediate Phases in $Na_{0.44}MnO_2$ for Sodium-Ion Battery. *Chem. Mater.* **2012**, *24*, 1205−1211.
(48) Van Der Ven, A.; Thomas, J. C.; Xu, Q.; Swoboda, B.; Morgan, D. Nondilute Diffusion from First Principles: Li Diffusion in Li_xTiS_2. *Phys. Rev. B: Condens. Matter Mater. Phys.* **2008**, *78*, 1−12.
(49) Rong, Z.; Malik, R.; Canepa, P.; Sai Gautam, G.; Liu, M.; Jain, A.; Persson, K.; Ceder, G. Materials Design Rules for Multivalent Ion Mobility in Intercalation Structures. *Chem. Mater.* **2015**, *27*, 6016−6021.
(50) Slingsby, J. G.; Rorrer, N. A.; Krishna, L.; Toberer, E. S.; Koh, C. A.; Maupin, C. M. Dynamic Free Energy Surfaces for Sodium Diffusion in Type II Silicon Clathrates. *Phys. Chem. Chem. Phys.* **2016**, *18*, 5121−5128.
(51) Chou, C. Y.; Kim, H.; Hwang, G. S. A Comparative First-Principles Study of the Structure, Energetics, and Properties of Li-M (M = Si, Ge, Sn) Alloys. *J. Phys. Chem. C* **2011**, *115*, 20018−20026.
(52) Zhao, K.; Wang, W. L.; Gregoire, J.; Pharr, M.; Suo, Z.; Vlassak, J. J.; Kaxiras, E. Lithium-Assisted Plastic Deformation of Silicon Electrodes in Lithium-Ion Batteries: A First-Principles Theoretical Study. *Nano Lett.* **2011**, *11*, 2962−2967.
(53) Stefanoski, S.; Martin, J.; Nolas, G. S. Low Temperature Transport Properties and Heat Capacity of Single-Crystal Na_8Si_{46}. *J. Phys.: Condens. Matter* **2010**, *22*, 485404.
(54) Stefanoski, S.; Beekman, M.; Wong-Ng, W.; Zavalij, P.; Nolas, G. S. Simple Approach for Selective Crystal Growth of Intermetallic Clathrates. *Chem. Mater.* **2011**, *23*, 1491−1495.
(55) Schäfer, M. C.; Yamasaki, Y.; Fritsch, V.; Bobev, S. Ternary Compounds in the Sn-Rich Section of the Ba−Ga−Sn System: $Ba_8Ga_{16-x}Sn_{30+x}$ ($1.1 \leq x \leq 2.8$) Clathrates of Type-I and Type-VIII, and $BaGa_{2-x}Sn_{4+x}$ ($x \approx 0.2$) with a Clathrate-like Structure. *Crystals* **2011**, *1*, 145−162.
(56) Horie, H.; Kikudome, T.; Teramura, K.; Yamanaka, S. Controlled Thermal Decomposition of NaSi to Derive Silicon Clathrate Compounds. *J. Solid State Chem.* **2009**, *182*, 129−135.
(57) Wan, W.; Zhang, Q.; Cui, Y.; Wang, E. First Principles Study of Lithium Insertion in Bulk Silicon. *J. Phys.: Condens. Matter* **2010**, *22*, 415501.
(58) He, Y.; Lu, X.; Kim, D. Y. A First-Principles Study on Si_{24} as an Anode Material for Rechargeable Batteries. *RSC Adv.* **2018**, *8*, 20228−20233.
(59) Ceder, G.; Ong, S. P.; Wang, Y. Predictive Modeling and Design Rules for Solid Electrolytes. *MRS Bull.* **2018**, *43*, 746−751.

DOI: 10.1021/acs.jpcc.9b06424
J. Phys. Chem. C 2019, 123, 22812−22822